Materials Today Bio 18 (2023) 100546

Contents lists available at ScienceDirect

Materials Today Bio

journal homepage: www.journals.elsevier.com/materials-today-bio

Barrier-penetrating liposome targeted delivery of basic fibroblast growth factor for spinal cord injury repair

Fenzan Wu [a,b,c], Penghui Wang [b], Xiaojie Wei [b], Yanhong Yang [c], Abdullah Al Mamun [c], Xie Zhang [d], Yunsen Zhu [a], Tingting Mo [a], Hongyu Zhang [a,b,c], Chang Jiang [a,***], Jie Hu [e,**], Jian Xiao [a,b,c,*]

[a] Department of Arthroplasty, The First People's Hospital of Wenling, Affiliated Wenling Hospital, Wenzhou Medical University, Zhejiang, 317500, China
[b] Translational Medicine Laboratory, Affiliated Cixi Hospital, Wenzhou Medical University, Zhejiang, 325300, China
[c] School of Pharmaceutical Sciences, Wenzhou Medical University, Zhejiang, 325035, China
[d] Department of Pharmacy, Ningbo Medical Treatment Center Li Huili Hospital, Zhejiang, 315040, China
[e] Stem Cell Translation Laboratory, Shanxi Bethune Hospital, Shanxi Academy of Medical Sciences, Tongji Shanxi Hospital, Third Hospital of Shanxi Medical University, Shanxi, 030032, China

ARTICLE INFO

Keywords:
Spinal cord injury
Liposome
Target
Basic fibroblast growth factor
Drug delivery

ABSTRACT

Nanoparticle technologies offer a non-invasive means to deliver basic fibroblast growth factor (bFGF) for the treatment of spinal cord injury (SCI). However, the inability of bFGF to accumulate at the injury site and inefficient penetration across the blood-spinal cord barrier (BSCB) remain challenges. The present study describes a dual-targeting liposome (bFGF@Lip-Cp&Rp) with injury lesion targeting and BSCB-penetrating capability to deliver bFGF for SCI treatment. The CAQK peptide (Cp) with injury lesion targeting ability and R_2KC peptide (Rp) with BSCB-penetrating capability were grafted onto the liposomes for a flexible and non-invasive drug delivery systems preparation. Results exhibit that the dual-targeted liposomes could significantly cross the BSCB and accumulate at the injury site. During the early stage of SCI, bFGF@Lip-Cp&Rp promotes repair of BSCB and facilitates M2-polarization of macrophages. Regular delivery of bFGF@Lip-Cp&Rp increase HUVECs tube formation and angiogenesis, ameliorate the microenvironment of lesion site, suppress the neuronal apoptosis and axonal atrophy in SCI rats. Importantly, continuous treatment of bFGF@Lip-Cp&Rp supports the restoration of limb motor function in SCI rats. In summary, this research implies that the injury site-targeting and BSCB-penetrating liposomes could be a promising therapeutic approach for the treatment of SCI.

1. Introduction

Spinal cord injury (SCI) is a severe neurological condition associated with irreversible loss of motor and sensory abilities [1]. The complicated pathological environment, including the disruption of blood spinal cord barrier (BSCB), severe reaction of inflammation, atrophy of axon, and apoptosis of neuronal makes the SCI difficult to recover [2,3]. Various approaches for the treatment of SCI have been explored including surgical decompression [4,5], rehabilitation training [6], neurotrophic support [7], cell implantation [8–11] and polymer skeleton transplantation [12–14]. Drug treatment is considered as the most promising approach to treating and managing SCI, which plays a crucial role in the entire clinical treatment regardless of acute or secondary injury stage. Previous studies suggest that basic fibroblast growth factor (bFGF),

Abbreviations: SCI, Spinal cord injury; BSCB, Blood-spinal cord barrier; bFGF, Basic fibroblast growth factor; CSPGs, Chondroitin sulfate proteoglycans; Cp, CAQK peptide; Rp, R_2KC peptide; ^{1}H NMR, ^{1}H Nuclear magnetic resonance; Mal, Maleimide; FITC-BSA, Fluorescein isothiocyanate-labeled bovine serum albumin; CCK-8, Cell counting kit-8; HUVECs, Human umbilical vein endothelial cells; VEGF-A, Vascular endothelial growth factor A; CD31, Platelet endothelial cell adhesion molecule-1; ZO-1, Zonulaoccludens 1; NGF, Nerve growth factor; NT-3, Neurotrophin-3; TGF-β, Transforming growth factor-β; IL-10, Interleukin 10; CD86, Cluster of differentiation 86; Arg-1, Arginase 1; NF-200, Neurofilament-200; GFAP, Glial fibrillary acidic protein; DSPE-PEG_{2000}, 1,2-distearoyl-*sn*-glycero-3-phosphoethanolamine-N-[methoxy(polyethylene glycol)-2000]; DiI, 1-dioctadecyl-3,3,3,3-tetramethylindocarbocyanine perchlorate; BBB, Basso-Beattie-Bresnahan.

* Corresponding author. School of Pharmaceutical Sciences, Wenzhou Medical University, Zhejiang, 325035, China.
** Corresponding author.
*** Corresponding author.
E-mail addresses: 595645040@qq.com (C. Jiang), hujie0811@163.com (J. Hu), xfxj2000@126.com (J. Xiao).

https://doi.org/10.1016/j.mtbio.2023.100546
Received 17 November 2022; Received in revised form 20 December 2022; Accepted 6 January 2023
Available online 7 January 2023

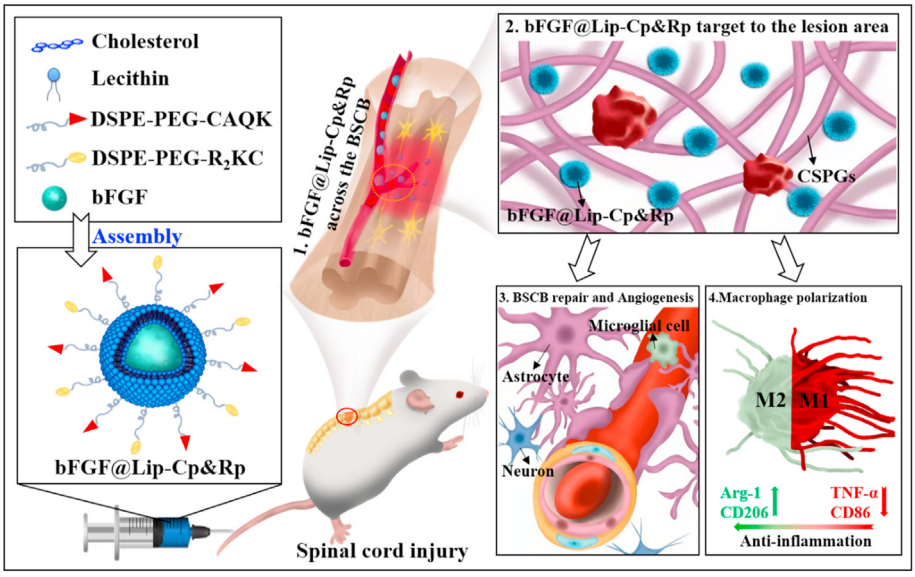

Fig. 1. Preparation and application of barrier-penetrating and injury-targeting liposomes (bFGF@Lip-Cp&Rp) for spinal cord injury (SCI) repair. bFGF@Lip-Cp&Rp were injected into the tail vein and crossed the blood-spinal cord barrier (BSCB), targeted to the lesion area to promote BSCB repair, angiogenesis and M2-type macrophage polarization.

expressed throughout the nervous system, promotes proliferation and mitosis of neuron, ameliorates the permeability of BSCB and regulates the stability of the microenvironment essential for SCI repair [12,15,16]. However, the promising therapeutic effect of bFGF is limited by poor stability, short half-life, complex structure and enzymatic inactivation [17,18].

Recently, numerous biomaterials have been developed for SCI treatment [2,8,19,20]. For example, a DNA supramolecular hydrogel with highly permeability was developed to promote neurogenesis and functional recovery after completely transected SCI [13]. Using peptide sequence mutations in nonbioactive monomers of amphiphilic monomers, Álvarez et al. developed bioactive scaffolds with an increased supramolecular motion that effectively promote recovery from SCI [12]. In addition, as a high-safety and effective drug delivery system, liposomes can encapsulate bFGF and prevent it from degradation by enzymes in the environment [21,22]. Besides, good biocompatibility, easy modification and preparation make liposomes as ideal bFGF delivery carrier [23,24]. However, due to non-specific toxicity and BSCB limitations [25], how to delivery bFGF to the SCI lesion site still remain challenge.

Growing evidence suggests that active targeting drug delivery system is one of the most promising therapeutic strategies to treating and managing SCI [26,27]. Chondroitin sulfate proteoglycans (CSPGs) are significant components of the extracellular matrix and crucial to the SCI recovery process by inhibiting neural regeneration or enclosing the damaged area [28,29]. As CSPGs substantially manifest at the site of injury within 24 h after the injury and can persist for several months [30,31], CSPGs-targeting strategies were extensively researched. Previous research shows that CAQK peptide (Cp) can selectively bound to CSPGs [28,32,33]. Although CAQK-modified liposomes were added into a thermosensitive heparin-poloxamer hydrogel (CAQK-LIP-GFs/DTX@HP) by our group for local administration therapy in SCI [34], single administration in situ can't repair long-term chronic SCI and a fixed therapeutic strategy cannot be adjusted flexibly according to the pathological characteristics of SCI. Therefore, systemic administration of Cp-modified liposomes which can deliver bFGF repeatably by non-invasive means maybe a good choice for SCI treatment. However, systemic delivery is often limited by the complex pathophysiological structure of SCI, especially by the BSCB, which prevents macromolecular drugs from reaching the spinal cord through circulation [2,35]. Multiple strategies have been explored to deliver potential therapeutic agents across BSCB including intranasal delivery [36], cell-penetrating transactivator of transcription peptide [37,38], triphenylphosphonium and apamin decoration of the nanoparticle surfaces [39–41]. Recent evidence indicates that the mitochondrion-targeted peptide (arginine-lysine, G2R) [42] and arginine-rich peptides facilitate crossing the cellular bilayer membrane by interacting with the cell membrane with negatively charged and induce enhanced membrane permeability [43,44]. So, we anticipated that the modification of liposome with CAQK and R_2KC would lead to a drug delivery system (bFGF@Lip-Cp&Rp) with increased BSCB permeability, drug delivery effectiveness, medication stability, and therapeutic efficacy.

Herein, we proposed a dual-targeting strategy, in which we developed an injury lesion-targeting and BSCB-penetrating delivery system (bFGF@Lip-Cp&Rp) for bFGF delivery (Fig. 1). Rp and Cp were grafted onto liposomes to prepare bFGF-loaded dual-targeting liposomes (bFGF@Lip-Cp&Rp). We speculated that Rp promoted the liposome crossing the BSCB, while Cp facilitated the liposome targeting and accumulating at SCI lesion. The excellent lesion targeting and BSCB-penetrating ability were verified using *in vitro* and *in vivo* experiments. Consequently, our findings indicate that bFGF@Lip-Cp&Rp may significantly promote the repair of BSCB, increase M2 type polarization of macrophage at the early stage of SCI. Regular delivery of bFGF@Lip-Cp&Rp increase the formation of microvascular, maintain the stability of the internal environment and suppress the apoptosis of neuronal and atrophy of axonal after SCI. In addition, bFGF@Lip-Cp&Rp treatment accelerate hind-limb motor function recovery. Due to good biocompatibility and excellent repairing effects of the liposomes, clinical applications might be anticipated.

2. Materials and methods

2.1. Materials

Soybean lecithin, cholesterol and chloroform-d were purchased from Aladdin Industrial Corporation (Shanghai, China). DSPE-PEG_{2000} and DSPE-PEG_{2000}-Mal were purchased from Xi'an Ruixi Biological

Technology Co., Ltd (Shanxi, China). CSPGs were obtained from Millipore (CC117, Billerica, MA, USA). The enhanced CCK-8 reagent was purchased from Beyotime Biotechnology (C0042, Jiangsu, China). FITC-BSA (SF063) and DiI (D8700) was purchased from Solarbio Technology Co., Ltd (Beijing, China). bFGF was purchased from Wenzhou Medical University (Zhejiang, China). FITC-phalloidin was purchased from Yeasen (40735ES75, Shanghai, China). Evans Blue (E2129) and FITC-dextran were purchased from Sigma-Aldrich, USA. Matrigel basement membrane maxtrix (356234) were purchased from Corning, USA. DMEM, FBS, penicillin-streptomycin solution, and 0.25% trypsin-EDTA were bought from Gibco, USA. The rabbit anti-Arg-1 (380744) and anti-CD86 (380350) antibodies were bought from Chengdu Zhengneng Biotechnology Co., Ltd. The rabbit anti-Occludin (27260-1-AP), rabbit anti-β-catenin (51067-2-AP), rabbit anti-ZO-1 (21773-1-AP), mouse anti-CD31 (66065-2-lg), rabbit anti-VEGF-A (R26073), mouse anti-β-actin (66009-1-lg) and rabbit anti-GAPDH (60004-1-lg) were bought from Proteintech. The mouse anti-CD206 (sc58986) was purchased from Santa Cruz, USA. GFAP antibody (#3670) was purchased from Cell Signaling Technology (Danvers, MA, USA). NF-200 antibody (ab4680), Anti-NeuN antibody (ab104225) and Alexa-conjugated secondary antibodies (ab150075, ab150113, ab150073) were purchased from Abcam (Cambridge, MA, USA).

2.2. Synthesis and characterization of DSPE-PEG-CAQK and DSPE-PEG-R_2KC

The sulfhydryl-maleimide coupling method was employed to synthesize the DSPE-PEG-R_2KC and DSPE-PEG-CAQK via covalent conjugation of the terminal sulfhydryl group of R_2KC or CAQK with DSPE-PEG-Mal [45]. Briefly, DSPE-PEG-Mal and CAQK/R_2KC peptide (1: 1.5, mol/mol) were dissolved in a buffer solution (pH 7.4) and gently stirred at 4 °C under nitrogen protection for 24 h. Subsequently, the residual CAQK/R_2KC peptide was removed by dialysis (1000 Da). Then, the DSPE-PEG-CAQK and DSPE-PEG-R_2KC were obtained by freeze-drying and ^{1}H NMR spectra were characterized using Oxford NMR AS400 spectrometer.

2.3. Liposomes preparation

As previously reported, peptide-modified liposomes were fabricated by thin-film hydration and membrane-filtering extrusion method [46]. For Lip-Cp&Rp as an example, soybean lecithin, cholesterol, DSPE-PEG-CAQK and DSPE-PEG-R_2KC (80: 20: 4: 4, molar ratio) were added to the around-bottomed flask and dissolved in chloroform/methanol (3:1, v/v) solution. A film was obtained after removing the solvent by rotary evaporation at 50 °C. Then, the dried film was hydrated with PBS (pH 7.4, 50 °C, 1 h). The Lip-Cp&Rp was fabricated by ultrasonication using a probe sonicator (JY92-IIN, Scientz) for 10 min (300 W, on/off: 2s/4s) followed by extrusion through membranes with a micropore size of 0.45 μm and 0.22 μm. The other peptide-modified liposomes were prepared using the same method, except different peptide-modified lipids were used. For bFGF loading, a pH gradient method was employed. Liposomes were adequately hydrated in citric acid buffer (0.03 mol/L) for 1 h and bFGF was added, followed by adjusting the pH to 6.8 using saturated disodium hydrogen phosphate solution and incubation at 35 °C for 15 min. Excessive bFGF was removed by dialysis, followed by ultrafiltration and centrifugation (20,000 Da molecular weight cut-off).

2.4. Liposomes characterization

The nanoparticle size, PDI, and zeta potential of liposomes were detected using a Litesizer particle analyzer (Litesizer 500, Anton Paar, Austria). Each sample was measured in triplicate. The stability of liposomes was assessed by measuring the size and zeta potential changes in PBS during storage. The bFGF content was determined using a human bFGF ELISA kit. The encapsulation efficiency was calculated as follows: Encapsulation efficiency (%) = actual bFGF loaded/theoretical bFGF loaded × 100%. Liposome morphology was determined using TEM (JEM 1200EX, JEOL, Japan). Briefly, 10 μL of liposomes was dropped onto a copper grid with 200-mesh and drained with filter paper. Then, 2% phosphotungstic acid was applied for 10 min as a negative stain and naturally dried for 2 days for detection.

2.5. Drug release tests

In vitro, drug release assays were conducted using a dialysis method. FITC-BSA, a fluorescence protein, was chosen to simulate the drug release of bFGF. Briefly, FITC-BSA@Lip solution (20 μg/mL, 2 mL) was placed into a dialysis bag (MWCO, 100 kDa) and released at 10 mL PBS (pH 7.4) medium at 37 °C. 500 μL of the liquid was removed and fresh PBS was replenished at 12 h, 1 d, 2 d, 3 d, 5 d, 7 d, 10 d and 14 d. The fluorescence intensity of FITC-BSA was measured using a multi-function microplate reader (Synergy NEO2, BioTek, USA) at 495 nm excitation light and 519 nm emission light. Finally, the cumulative release was calculated.

2.6. Cell cytotoxicity analysis

Cytotoxicity was measured in PC12 and bEnd. 3 cells using CCK-8 cell proliferation assay. Briefly, 100 μL of cell suspensions were added into 96-well plates at 3×10^4 cells/mL; bFGF at 0.5, 1, 5, 10, 20 and 50 μg/mL and the liposome preparations (Lip, bFGF@Lip, bFGF@Lip-Cp, bFGF@Lip-Rp, or bFGF@Lip-Cp&Rp) (equivalent to 10 μg/mL of bFGF) were added and cultured with cells for 48 h. Then, 100 μL of culture medium with 10% CCK-8 solution was replaced and left for 2 h. The absorbance rate was finally measured at 450 nm using a microplate reader (BioTek, USA).

2.7. Hemolysis analysis

The hemolytic potential of various concentrations and types of liposomes was measured using red blood cells [47]. Briefly, fresh blood was collected from female Sprague Dawley rat hearts and placed in anti-coagulant tubes. The blood was washed adequately with physiological saline and centrifuged (2000 rpm, 10 min) repeatedly. The 2% red blood cell suspensions were prepared and mixed with various concentrations and types of liposomes at a 1:1 vol ratio. The mixture was centrifuged (2000 rpm, 10 min) after 3 h incubation and 200 μL of the supernatants were removed to measure the hemoglobin content at 576 nm using a microplate reader. Normal saline and 1% Triton solution were employed as negative and positive controls, respectively.

2.8. Barrier-penetrating and injury-targeting test

The BSCB model *in vitro* was constructed by using the Transwell system (Corning Costar, Corning, NY, USA). Briefly, HUVECs (1×10^5 cells/chamber) were seeded into the Transwell's upper chamber for 2 days with a medium containing 10% FBS and serum-starved for another 1 day with 10^3 nmol/L of hydrocortisone to increase the tightness of the barrier. CSPGs were coated onto the lower chamber of Transwell chambers overnight and adequately washed twice before adding to the upper chamber seeded with HUVECs. Then, 100 μL of DiI-loaded liposomes (20 μg/mL of DiI) or BSA-FITC-loaded liposomes (50 μg/mL of BSA-FITC) were added into the top chamber with 700 μL of fresh medium in the lower chamber. 100 μL of culture medium from the lower chamber was then collected to measure fluorescence intensity after 3 h incubation. Human neuroblastoma cells (SHSY5Y) were cultured in the lower chamber of Transwell chambers instead of CSPGs to measure the fluorescence uptake of SHSY5Y cells. 100 μL of DiI-loaded liposomes (20 μg/

mL of DiI) were added to the upper chamber. After 12 h of culture, the cytoskeleton was stained with phalloidin, and DiI-loaded liposomes ingested by the SHSY5Y cells were measured using a confocal microscope (Nikon, Japan). The Small Animal *in vivo* Imaging System (MaestroCRI, MA USA) was employed to analyze the injury-targeting and barrier-penetrating effects of the liposomes in the SCI rat model. DiI-loaded liposomes were intravenously injected after SCI and measured at 6 h, 12 h and 24 h. The rat heart, liver, spleen, lung, kidney and spinal cord were harvested and subjected to fluorescence imaging.

2.9. Tube formation experiment

Matrigel was pre-coated on the bottom of a 96-well plate before being liquefied at 4 °C and gelled for 30 min at 37 °C. HUVECs were first incubated with PBS, bFGF@Lip, bFGF@Lip-Cp, bFGF@Lip-Rp, or bFGF@Lip-Cp&Rp for 4 h, and then 50,000 cells/well were added to the 96-well plate paved with matrigel. At 2 and 4 h time points, the cultured cells were observed and photographed. The results were detected by Image J.

2.10. SCI model and treatment

One hundred and sixty Sprague Dawley rats (female, average weight 200–220 g) were purchased from Weitong Lihua Laboratory Animal Technology Co., Ltd and housed at Wenzhou Medical University, Zhejiang Province. The experimental procedures and caring of the animals have complied with the Ethics Committee of Experimental Animals of Wenzhou Medical University (No.wydw2020-0313). The rats were allocated into six groups: Sham (animals underwent laminectomy without contusion injury), SCI + 0.9% NaCl, SCI + bFGF@Lip, SCI + bFGF@Lip-Cp, SCI + bFGF@Lip-Rp and SCI + bFGF@Lip-Cp&Rp. The rats were fasted overnight before surgery and anesthetized. A T-8 laminectomy was performed and contusion injury was constructed using a MASIS impactor dropped from the height of 50 mm [48]. Then, 0.5 mL liposomes (equivalent to 10 μg/mL of bFGF) were tail vein injected weekly until the end of the experiment. Manual bladder voiding was performed two times every day until urination was repaired.

2.11. Function behavior evaluation

Motor function recovery was assessed using the BBB scoring system. Two observers evaluated and recorded the hind-limb scores at 1, 3, 7, 14, 21 and 28 days after SCI. Hind-limb gait was assessed using footprint blotting at 28 days. The hind limbs were painted with red ink and placed on the narrow track (0.08 m width × 1 m length) with white paper. The footprints were then recorded and scanned.

2.12. Quantitative real-time polymerase chain reaction

QRT-PCR was employed to measure relative mRNA expression level. The TransZol Up reagent (TransGen, Beijing, China) was used to extract total RNA from rat T8 spinal cord tissues according to the supplier's instructions. For mRNAs, complementary DNA (cDNA) was constructed using a reverse transcription kit (TransGen, Beijing, China). Perfect Start Green qPCR SuperMix (TransGen, Beijing, China) was employed for qRT-PCR using the CFX96 RT-PCR (BioRad, Hercules, CA, USA) as described previously [49]. The specific primer sequences were as follows: rat NGF forward primer, TGCATAGCGTAATGTCCATGTTG and reverse primer, TGTGTCAAGGGAATGCTGAAGT; rat NT-3 forward primer, GACACAGAACTACTACGGCAACAG and reverse primer, ACTCTCCTCGGTGACTCTTATGC; IL-10 forward primer, GACAACATACTGCTGACA GATTCCT and reverse primer, TCACCTGCTCCACTGCCTTG; TGF-β1 forward primer, TGCGCCTGCAGAGATTCAAG and reverse primer AGGTAACGCCAGGAATTGTTGCTA. GAPDH forward primer, TGGAGTCTA CTGGCGTCTT and reverse primer, TGTCATATTTCTCGTGGTTCA. Relative mRNA expression was calculated using the 2-ΔΔCt method.

2.13. Histology and immunofluorescence staining

Injured spinal cord tissues (1 cm in length along the long axis) were embedded and sectioned at the 5-μm size. Nissl staining was applied to detect the Nissl bodies in the anterior horn of the spinal cord. In addition, HE staining was employed to assess the morphology of the injured tissue. Immunofluorescence staining of tissue sections for CD206 (1:100), CD86 (1:100), NeuN (1:1000), CD31 (1:200), ZO-1 (1:200), β-catenin (1:200), NF-200 (1:10,000), and GFAP (1:500) was conducted according to the previous method. Briefly, paraffin sections were adequately blocked with 5% BSA and inoculated with primary antibodies overnight at 4 °C. Then secondary antibodies (1:1000) conjugated to Alexa Fluor 488 or 647 were used to label the sections and the sections were mounted with DAPI-containing mounting fluid (Solarbio, Beijing, China). FITC-Phalloidin was added together with the secondary antibodies if applied. Finally, the sections were observed under a laser scanning confocal microscope (Nikon, Tokyo, Japan). The cavity area and fluorescence intensity were calculated using Image J software.

2.14. Statistical analysis

Data for quantitative analyses were presented as means and standard deviations. Analyses of the results were conducted with one-way ANOVA followed by Tukey's multiple comparisons test. When BBB scores analyses were required, a two-way ANOVA comparison test was used. $P < 0.05$ was considered statistically significant in all experiments. More than three replications of each experiment were conducted, and the results were representative.

3. Results and discussion

3.1. Preparation and characterization of bFGF@Lip-Cp&Rp

To prepare the injury-targeting and barrier-penetrating liposomes, target peptide (Cp) and transmembrane peptide (Rp) were coupled with DSPE-PEG-Maleimide (DSPE-PEG-Mal) (Fig. 2A). The ^{1}H NMR spectrum displayed that the characteristic peaks of the Mal group in DSPE-PEG-Mal at 6.7 ppm disappeared after DSPE-PEG-Mal was coupled with Cp and Rp, while the DSPE and PEG segments still presented at 1.2 ppm and 3.7 ppm, respectively (Fig. 2B). The results indicated the successful synthesis of DSPE-PEG-CAQK and DSPE-PEG-R_2KC. Then, the DSPE-PEG, DSPE-PEG-CAQK, or DSPE-PEG-R_2KC with lecithin and cholesterol were applied to prepare modified liposomes (Lip), injury-targeting liposomes (Lip-Cp), barrier-penetrating liposomes (Lip-Rp) and dual-modified liposomes (Lip-Cp&Rp). Dynamic light scattering revealed that Lip-Cp&Rp had an average particle size of 97.51 ± 0.78 nm. The results exhibited that the polydispersity index (PDI) was 0.191 ± 0.01 and the average zeta potential was −2.63 ± 0.64 mV (Fig. 2C). Similar particle size, PDI and zeta potential were significantly observed for Lip, Lip-Cp and Lip-Rp (Fig. S1). TEM revealed that the liposomes were in uniform sphere morphologies with bilayer structure (Fig. 2C). Significantly, the particle size and zeta potential of the Lip-Cp&Rp slightly changed after two weeks, indicating excellent stability (Fig. 2D). bFGF was encapsulated into liposomes (bFGF@Lip-Cp&Rp) with an entrapment efficiency of 90.83 ± 2.81% (Fig. S2). To measure the drug release of the liposomes, a FITC-BSA was selected to replace bFGF. Fig. 2E displays that BSA-FITC was slowly released in two weeks, reaching approximately 91.7 ± 5.36% and 82 ± 10.94% for bFGF@Lip and bFGF@Lip-Cp&Rp at 14d, respectively. These findings ensure that this slow and sustained release behavior regulates effective drug accumulation at the SCI lesion area.

Mounting evidence explains that biocompatibility is considered an

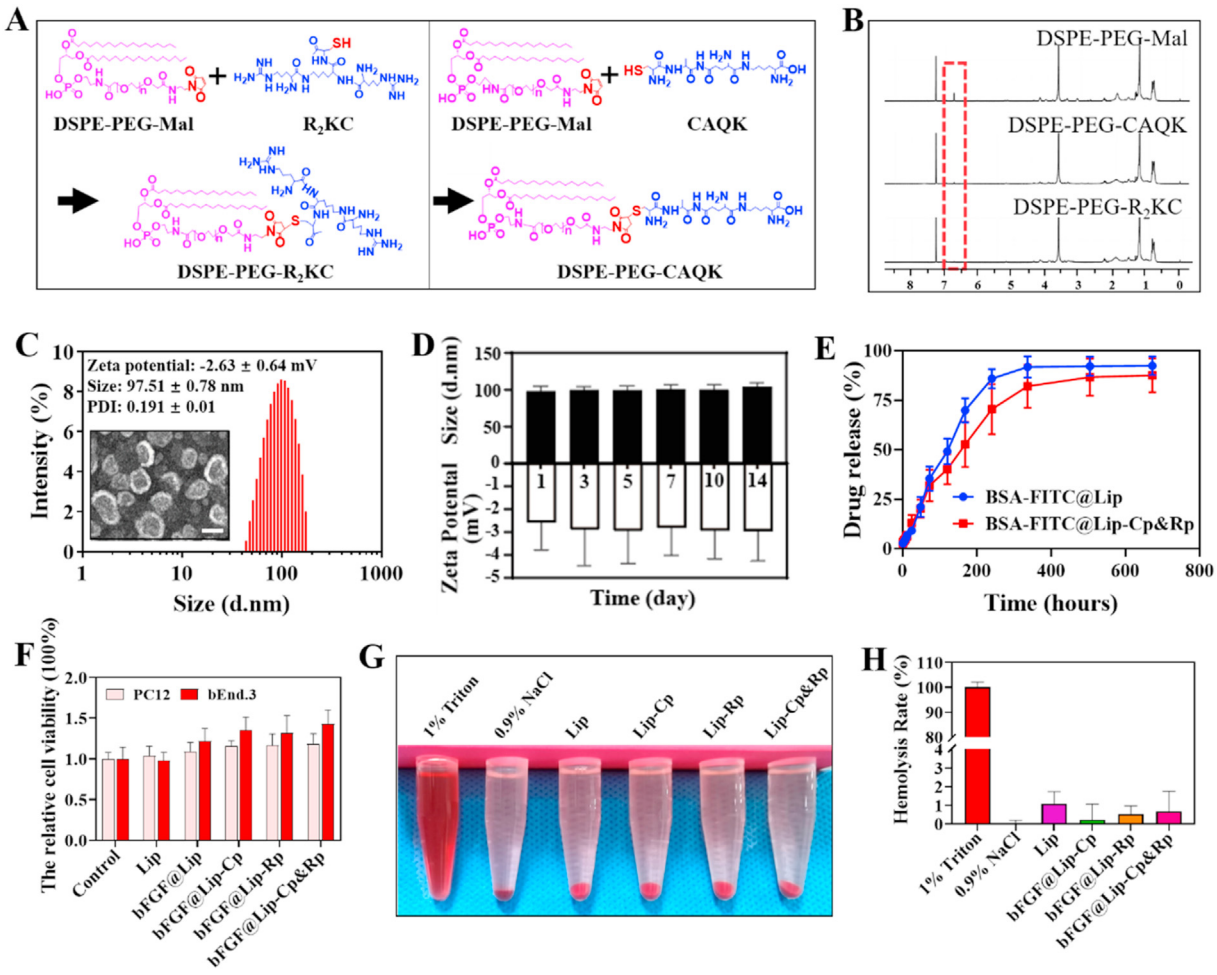

Fig. 2. Preparation and characterization of dual-modified liposomes (bFGF@Lip-Cp&Rp). (A) The synthesis routine of DSPE-PEG-R_2KC and DSPE-PEG-CAQK. (B) ^{1}H NMR spectrum of DSPE-PEG-Mal, DSPE-PEG-CAQK and DSPE-PEG-R_2KC in $CDCl_3$. (C) The representative size distribution and transmission electron microscope image of Lip-Cp&Rp, with the information of hydrodynamic radius, polydispersity index and zeta potential. The scale bar is 50 nm. (D) Particle size and zeta potential changes of Lip-Cp&Rp in 14 days. (E) The release profile of fluorescein isothiocyanate-labeled bovine serum albumin (FITC-BSA) in Lip and Lip-CP&Rp. (F) The viability of PC12 and bEnd.3 cells were cultured with different liposomes for 2 days. (G) The hemolytic activity of red blood cells incubated with different liposomes. 1% Triton and 0.9% NaCl serve as the positive and negative control, respectively. (H) Hemolysis rates of different liposomes. (For interpretation of the references to color in this figure legend, the reader is referred to the Web version of this article.)

excellent characteristic of liposomes for clinical applications [37]. Therefore, we analyzed the biocompatibility of the liposomes using a CCK-8 kit. The blank liposomes (Lip group) could not markedly affect PC12 or bEnd.3 cell viability while bFGF or bFGF loaded liposomes slightly promote cell proliferation at 24 h, 48 h, and 72 h (Fig. 2F and S3). Liposomes were further assessed for their biocompatibility using *in vitro* hemolysis tests. As shown in Figs. 2G and 1% Triton caused hemolysis while the different modified liposomes had no evident hemolysis effect, similar to normal saline; 1% Triton was a positive control and set as 100% hemolysis. The hemolysis rate of different liposomes was remarkably lower than 1.1% and was considered non-hemolysis (Fig. 2G). Interestingly, higher concentrations of liposomes caused no evident hemolysis (Figs. S4A and B). Collectively, these findings ensure the substantial biosafety and excellent biocompatibility of the liposomes.

3.2. bFGF@Lip-Cp&Rp penetrates the BSCB and targets the SCI lesion

To determine the BSCB penetrating and CSPGs targeting capability of Lip-Cp&Rp *in vitro*, we cultured HUVECs in the upper chamber of Transwell chambers as a BSCB model and covered a layer of CSPGs in the lower chamber. Two fluorescent substances (BSA-FITC as a water-soluble drug or DiI as a fat-soluble drug) were loaded into the liposomes and added to the upper chamber. The fluorescence in the lower chamber was measured 3 h later (Fig. 3A). The liposomes with targeting peptide (BSA-FITC@Lip-Cp/DiI@Lip-Cp) and penetrating peptide (BSA-FITC@Lip-Rp/DiI@Lip-Rp) had higher penetration ability than unmodified liposomes (BSA-FITC@Lip/DiI@Lip) and the dual-modified liposomes (BSA-FITC@Lip-Cp&Rp/DiI@Lip-Cp&Rp) had the highest fluorescence intensity (Fig. 3B–C). SHSY5Y cells were cultured in the lower chamber instead of CSPGs to determine the capability of DiI@Lip-Cp&Rp entering the SHSY5Y cells crossing through the upper chamber after 12 h of culture. The fluorescence images and semi-quantitative results revealed that the liposomes entering cells were remarkably enhanced in the DiI@Lip-Cp and DiI@Lip-Rp groups and the DiI@Lip-Cp&Rp group had the highest fluorescence intensities (Fig. 3D–E). Taken together, these findings imply that the dual-modified liposomes have a relatively excellent ability to cross the BSCB and penetrate cells.

The systemic side-effects of drugs might be alleviated while the drug is directly targeted and long-term retained in the lesion area through intravenous administration. To evaluate the SCI lesion targeting effect of Lip-Cp&Rp, DiI-loaded liposomes were intravenously injected and we then performed small-animal fluorescence imaging in the injury site at 6 h, 12 h and 24 h. The fluorescence and tissue distribution images revealed that the fluorescence accumulated in the lesion area rarely at 6 h

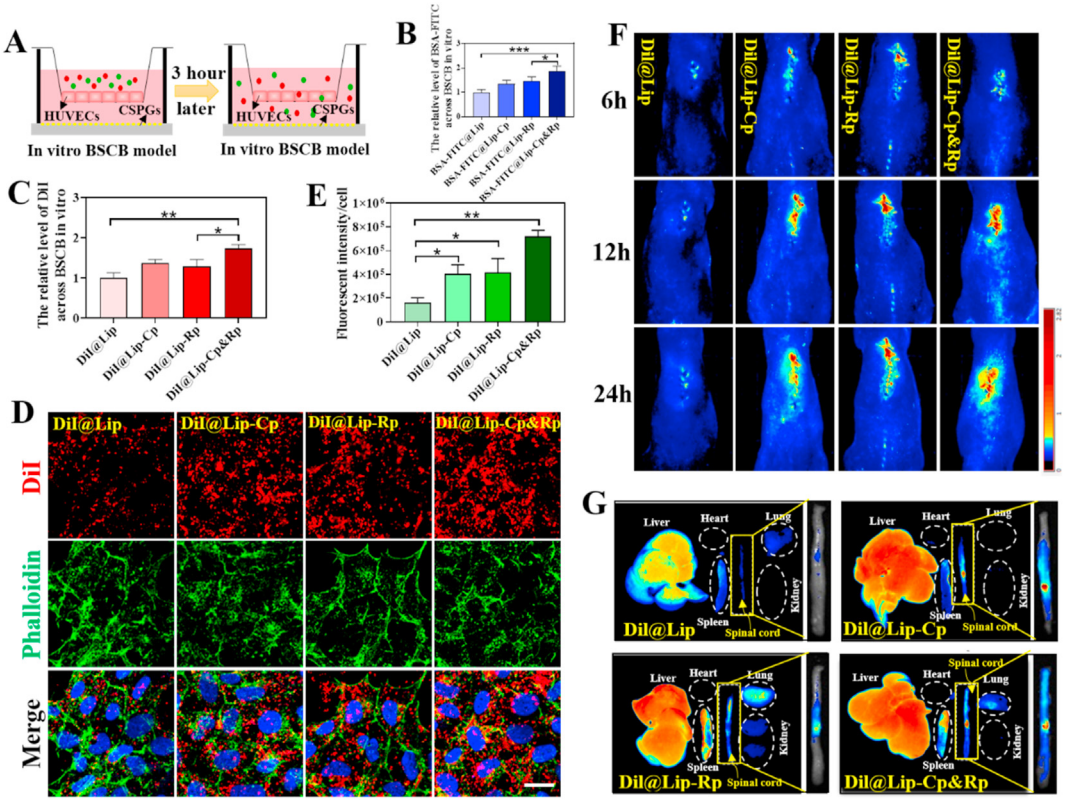

Fig. 3. The barrier-penetrating and injury-targeting effect of bFGF@Lip-Cp&Rp *in vitro* and SCI rat. (A) Schematic illustration of BSA-FITC@Lip-Cp&Rp or 1,1′-dioctadecyl-3,3,3′,3′-tetramethylindocarbocyanine perchlorate (DiI)@Lip-Cp&Rp pass through the barrier and target chondroitin sulfate proteoglycans (CSPGs) at the Transwell level. (B, C) The radio of BSA-FITC or DiI passes through the upper chamber of the Transwell chamber. (D) Fluorescence image of DiI-encapsulated liposomes passing through the upper chamber of the Transwell and entering the cells in the lower chamber. The scale bar is 25 μm (E) Semi-quantitative analysis of fluorescence intensity in image d. (F) Animal fluorescence imaging *in vivo* at 6 h, 12 h, and 24 h after tail-vein injection of DiI-loaded liposomes. (G) *Ex vivo* fluorescence imaging of heart, liver, spleen, lung, kidney, and spinal cord.

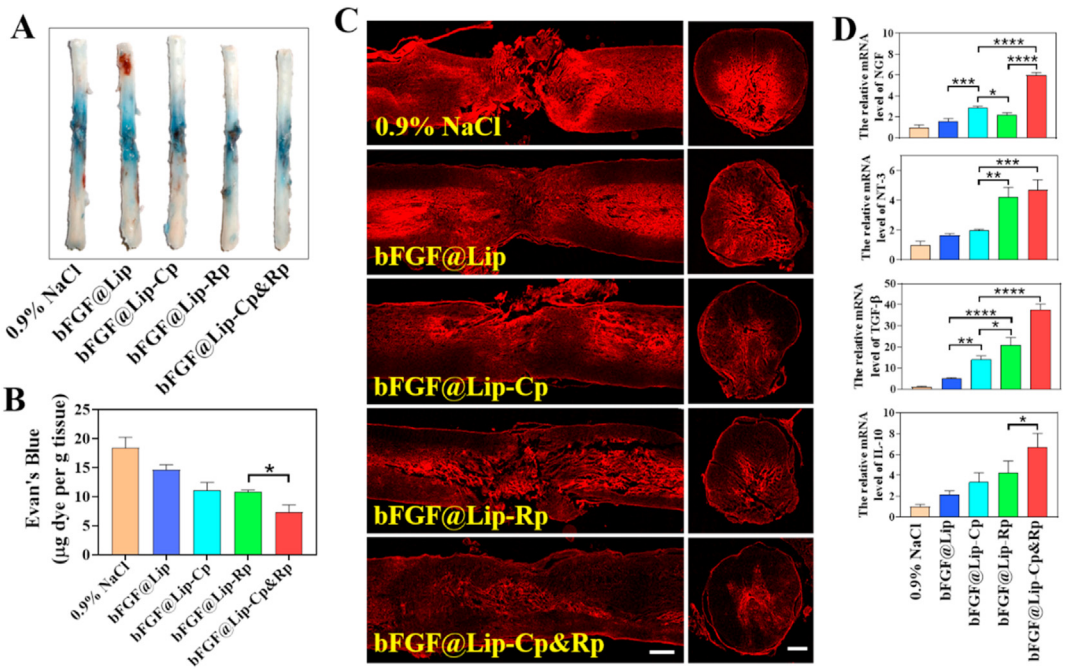

Fig. 4. Administration of bFGF@Lip-Cp&Rp restored the BSCB permeability and ameliorated the lesion microenvironment after SCI. (A) Representative images of SCI tissues injected with Evans blue 24 h after SCI. (B) Statistical results of Evans blue staining in SCI tissue 24 h after SCI. (C) Representative confocal images of SCI tissue sections with Evans blue tail-vein injection. Scale bars are 500 μm. (D) mRNA levels of neurotrophic factors such as nerve growth factor (NGF) and neurotrophin-3 (NT-3) and anti-inflammatory factor transforming growth factor-β (TGF-β) and interleukin 10 (IL-10) 3 days after SCI (n = 3 per group). (For interpretation of the references to colour in this figure legend, the reader is referred to the Web version of this article.)

after SCI, gradually increasing at 12 h and 24 h (Fig. 3F). Intriguingly, the DiI@Lip-Cp&Rp group had a most significant fluorescence aggregation than DiI@Lip-Cp and DiI@Lip-Rp group. Additionally, the DiI@Lip group had scant fluorescence aggregation. After *in vivo* fluorescence imaging,

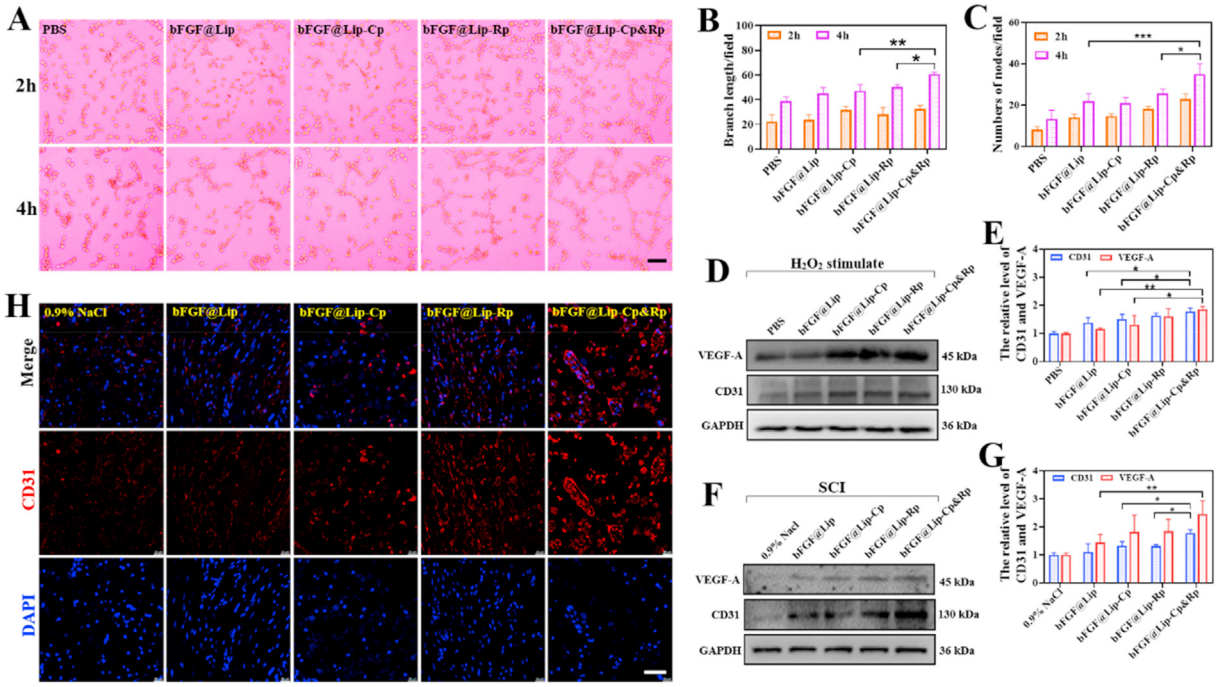

Fig. 5. bFGF@Lip-Cp&Rp promoted tube formation of HUVECs and angiogenesis. (A) Representative images of tube formation of HUVECs treated with different liposomes. HUVECs were pretreatment with different liposomes for 4 h before being transferred to matrigel for 2 and 4 h of culture. The scale bar is 200 μm. (B, C) Quantified analysis of the branch length and nodes numbers of tubes at 2 h and 4 h. At least three views in each group were analyzed. (D, E) Expression and quantification of VEGF-A and CD31 proteins of the HUVECs after H_2O_2 stimulation and liposomes treatment. (F, G) Expression and quantification of VEGF-A and CD31 proteins of the spinal cord tissue 14 days after SCI. (H) Representative immunofluorescence images of CD31 (red) and DAPI (blue) of the spinal cord tissue 14 days after SCI. The scale bar is 50 μm. (For interpretation of the references to colour in this figure legend, the reader is referred to the Web version of this article.)

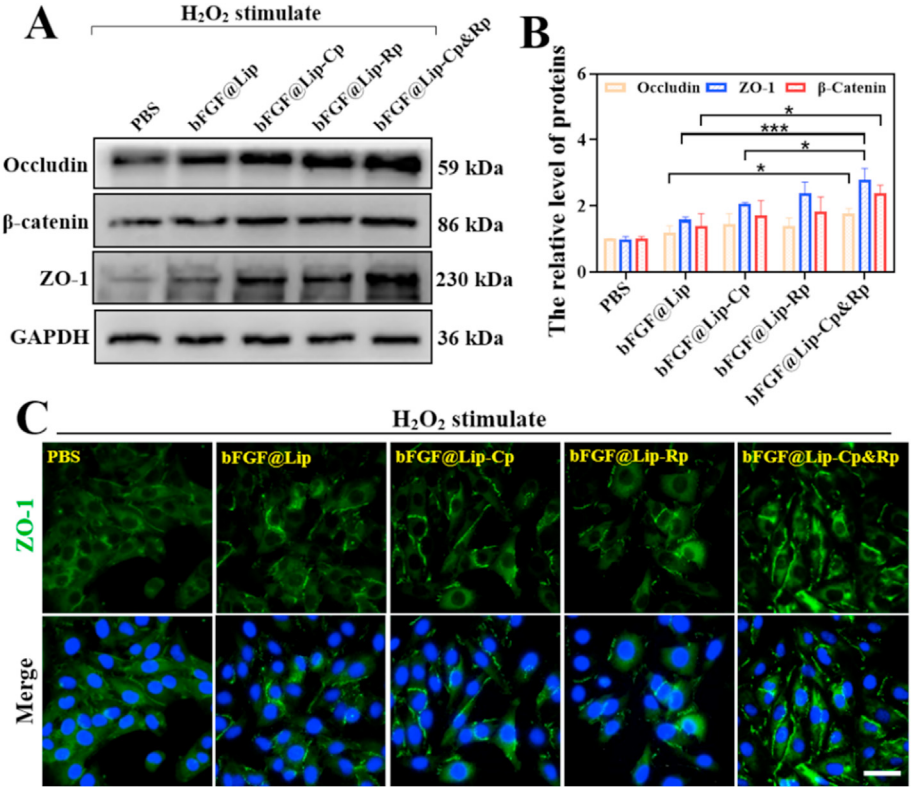

Fig. 6. bFGF@Lip-Cp&Rp promoted the expression of junction proteins in HUVECs. (A, B) Expression and quantification of Occludin, β-catenin and ZO-1 of the HUVECs after H_2O_2 stimulation and liposomes treatment. (C) Representative immunofluorescence images of ZO-1 (green) and DAPI (blue) of the HUVECs 1 day after H_2O_2 stimulation and liposomes treatment. The scale bar is 50 μm. (For interpretation of the references to colour in this figure legend, the reader is referred to the Web version of this article.)

the spinal cord, heart, liver, spleen, lung and kidney were removed immediately. Tissue distribution experiments revealed that the fluorescence intensity of the DiI@Lip-Cp&Rp group at the lesion area was higher compared to the DiI@Lip-Cp, DiI@Lip-Rp and DiI@Lip groups (Fig. 3G). Collectively, these findings indicate that bFGF@Lip-Cp&Rp accumulates at the target area after SCI.

3.3. bFGF@Lip-Cp&Rp promotes BSCB repair and enhances environment stability after SCI

The BSCB is damaged after physical trauma, allowing several external substances (including macrophages) to enter spinal cord lesions and destroy the stability of the microenvironment [28]. We injected rats with Evans blue dye to evaluate whether bFGF-loaded liposomes promote BSCB repair. The 0.9% NaCl group exhibited the highest blue dye after SCI due to BSCB destruction and Evans blue extravasation (Fig. 4A–B). The intervention of bFGF-loaded liposomes (bFGF@Lip, bFGF@Lip-Cp, bFGF@Lip-Rp and bFGF@Lip-Cp&Rp) significantly promoted BSCB repair with reduced Evans blue dye extravasation. The bFGF@Lip-Cp&Rp exhibited the most substantial BSCB repair ability. The BSCB repairing ability of bFGF-loaded liposomes was further analyzed by fluorescence imaging. The fluorescence intensity of Evans blue in the spinal cord was reduced after bFGF@Lip-Cp&Rp treatment in the cross and longitudinal sections (Fig. 4C). Previous studies indicate that bFGF ameliorates the SCI microenvironment, which delivers a promising therapeutic avenue for treating and managing SCI. The nutritional factors such as NGF and NT-3 and anti-inflammatory factors TGF-β and IL-10 were measured to evaluate the promising impact of bFGF-loaded liposomes on the local microenvironment of SCI. The mRNA levels of NGF, NT-3, TGF-β and IL-10 were markedly elevated in the bFGF@Lip-Cp&Rp-treated group (Fig. 4D). Collectively, these findings imply that the dual targeting drug-delivery strategy allows bFGF to target SCI lesions by sustained release behavior to facilitate BSCB repair and environment stability.

3.4. bFGF@Lip-Cp&Rp increases angiogenesis and tight-junction protein expression

Vascular dysfunction is the primary factor of the inimical injury microenvironment that result in neuron death and axonal atrophy. While angiogenesis is an essential requirement for replenishing the blood and oxygen supply [50], it is also a major therapy obstacle for SCI [51]. *In vitro*, the effect of bFGF@Lip-Cp&Rp on HUVECs tube formation was observed. Result showed that the length of branches and the number of nodes is most in the bFGF@Lip-Cp&Rp pretreatment group than in other monomodified or unmodified liposomes (Fig. 5A–C). In addition, the quantity of vascular endothelial growth factor A (VEGF-A) and neovascular factor platelet endothelial cell adhesion molecule-1 (CD31) were detected by western blot and immunofluorescence. The result showed that bFGF@Lip-Cp&Rp treated group had the highest expression of VEGF-A and CD31 compared with the other groups after stimulation (Fig. 5D–E). *In vivo*, the protein expression of VEGF-A and CD31 was also detected 14 days after SCI and the bFGF@Lip-Cp &Rp treated group had the highest expression (Fig. 5F–G). The same result was observed by

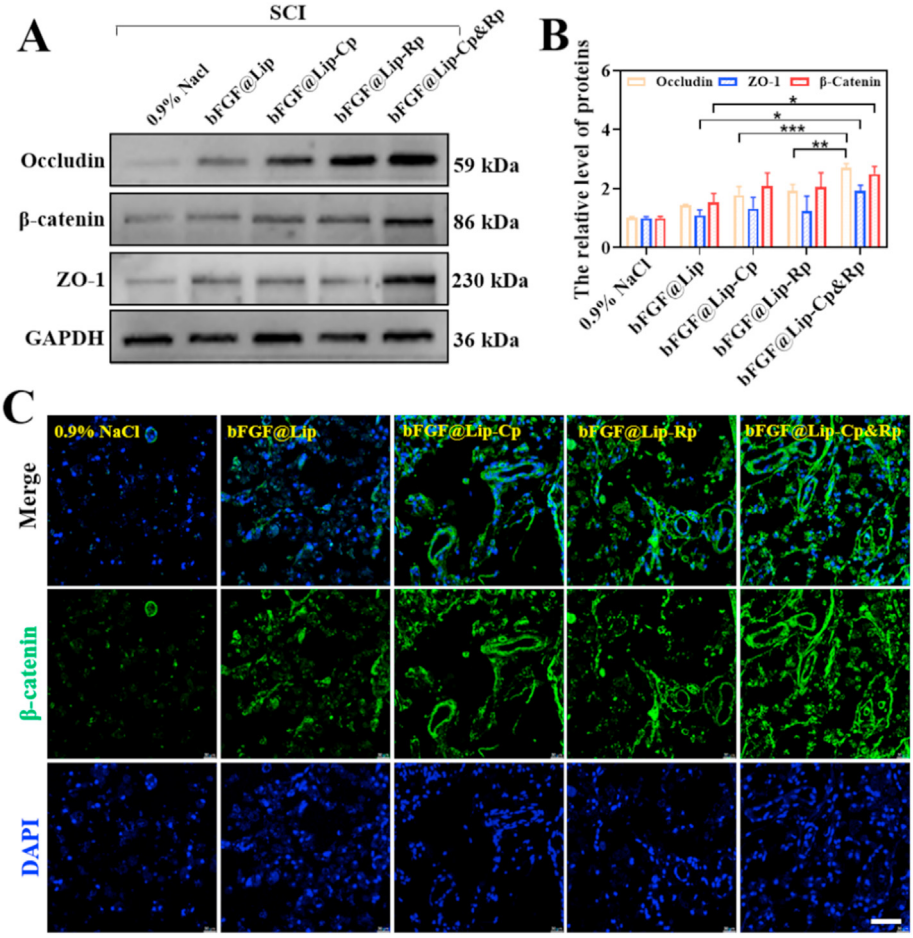

Fig. 7. bFGF@Lip-Cp&Rp promoted the expression of junction proteins in spinal cord tissue. (A, C) Expression and quantification of Occludin, β-catenin and ZO-1 proteins of the spinal cord tissue 1 day after SCI. (C) Representative immunofluorescence images of β-catenin (green) and DAPI (blue) of the spinal cord tissue after SCI. The scale bar is 50 μm. (For interpretation of the references to colour in this figure legend, the reader is referred to the Web version of this article.)

using CD31 immunofluorescence (Fig. 5H) that the bFGF@Lip-Cp&Rp administration group had the highest fluorescent intensity. In addition, to support the repair of the BSCB, tight junction protein also enhances the integrity of newly formed blood vessels which were made up of microvessel endothelial cells. As shown in Fig. 6A-C, the expression of tight junction proteins (Occludin, β-catenin, ZO-1) was highest and the fluorescent intensity of ZO-1 was strongest in the bFGF@Lip-Cp&Rp treated group *in vitro*. A similar result was obtained *in vivo* by detecting junction protein expression 1 day after SCI. Western blot analysis showed that bFGF@Lip-Cp&Rp treatment induce the most highly expression of Occludin, β-catenin and ZO-1 among them. Immunofluorescence staining also showed that β-catenin protein was most abundantly expressed after bFGF@Lip-Cp&Rp treatment (Fig. 7A–C).

3.5. bFGF@Lip-Cp&Rp increases M1 to M2 phenotype macrophage transformation

After SCI, macrophages accumulate at the lesion site, leading to a severe inflammatory response [52]. Macrophage phenotype transformation from M1 (pro-inflammatory) to M2 (anti-inflammatory) is critical for damage repair [50,53]. Anti-inflammatory factors TGF-β and IL-10 were significantly augmented after bFGF-loaded liposomes treatment. In our research, we speculated that the elevated anti-inflammatory factors might be due to the M2-type polarization of macrophages. Therefore, we evaluated the therapeutic effects of different bFGF-loaded liposomes on M1 and M2 phenotype changes in the lesion area after SCI (Fig. 8A). The results exhibited that the expression level of Arg-1 (an M2 marker) was up-regulated and CD86 (an M1 marker) was down-regulated after bFGF@Lip treatment. bFGF@Lip-Cp and bFGF@Lip-Rp treatment could markedly enhance the promising effect. More importantly, administration of bFGF@Lip-Cp&Rp after SCI significantly up-regulated the expression of Arg-1 protein and downregulated the expression of CD86 protein (Fig. 8B–C). We next measured the expression levels of CD86 and CD206 (an M2 marker) in SCI lesions using fluorescence staining. We found many pro-inflammatory cells (red) in the lesion area in the 0.9% NaCl group with a less (green) expression of anti-inflammatory macrophages. After bFGF@Lip treatment, the expression level of CD86 was downregulated and the expression level of CD206 was up-regulated, suggesting an M1-to-M2 phenotype switch with the targeting peptide (Cp) and penetrating peptide (Rp) attached to

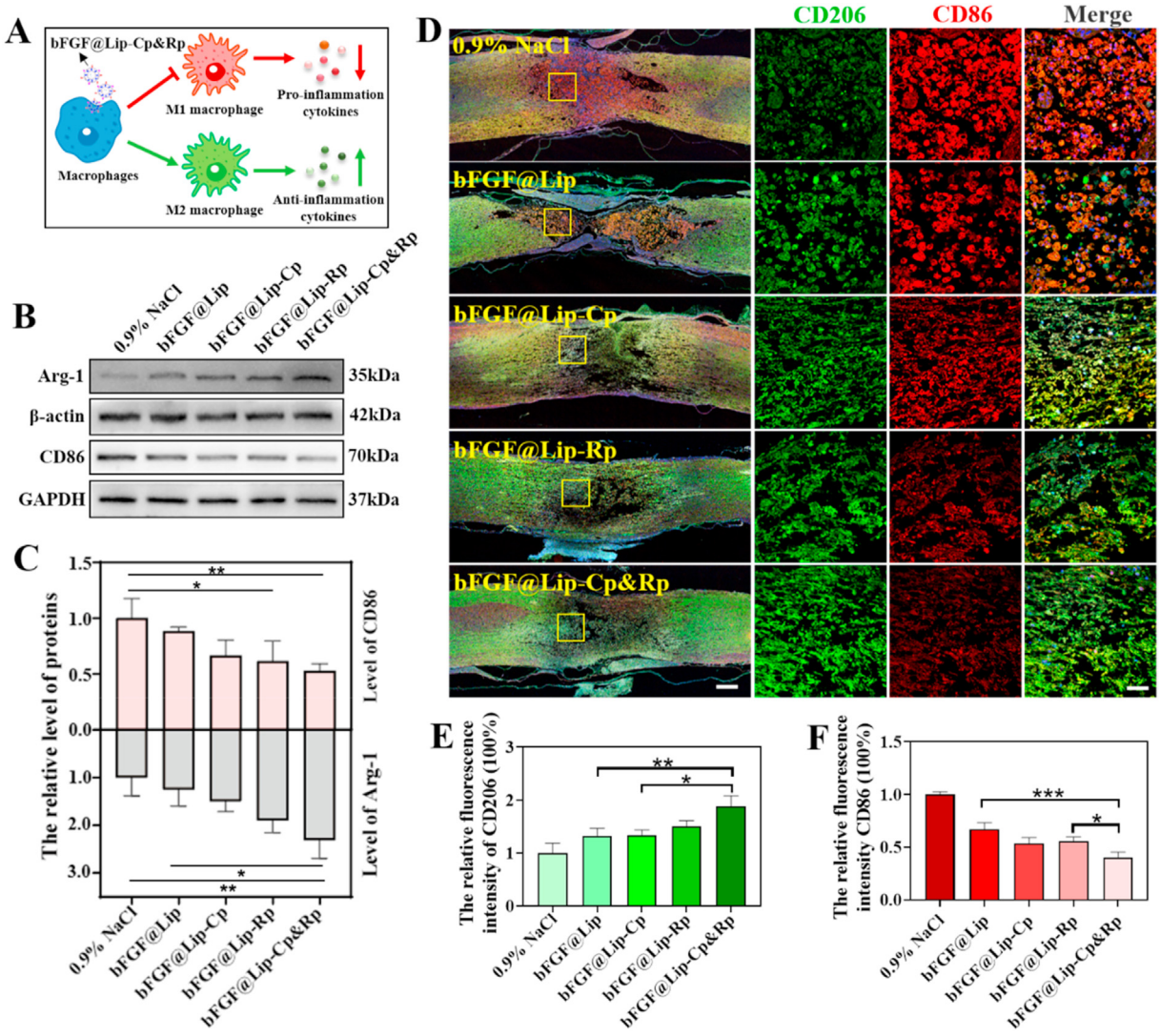

Fig. 8. bFGF@Lip-Cp&Rp promoted the transformation of macrophages to M2 type and inhibited to M1 type. (A) Schematic of bFGF@Lip-Cp&Rp in macrophage phenotype transformation and inflammatory factors expression. (B, C) Expression and quantification of arginase-1 (Arg-1) and CD86 3 days after SCI. (D) Representative immunofluorescence images of CD206 (green) and CD86 (red) of the spinal cord tissue 3 days after SCI. The scale bar is 500 μm in rectangle images and 50 μm in square images. (E, F) Semi-quantitative analysis of the relative fluorescence intensity of CD206 (green) and CD86 (red) according to immunofluorescence image D. (For interpretation of the references to colour in this figure legend, the reader is referred to the Web version of this article.)

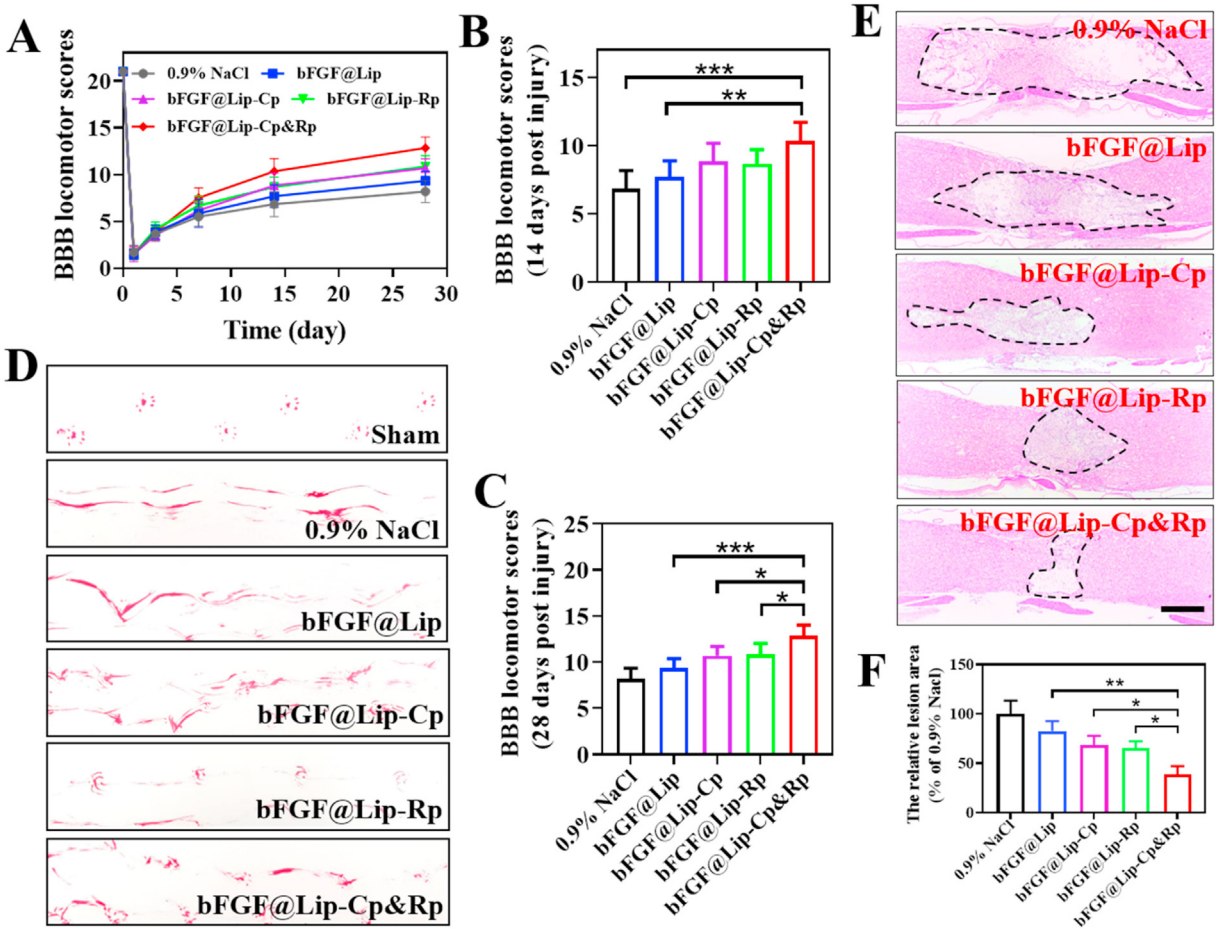

Fig. 9. bFGF@Lip-Cp&Rp promotes motor function and injury tissue repair after SCI. (A) Basso-Beattie-Bresnahan locomotion scores of different groups. (B–C) BBB locomotion score of different groups at 14 days and 28 days. (D) Representative footprint images of different groups 28d after SCI. (E) Representative hematoxylin and eosin (HE) staining images at 28d after SCI. The scale bar is 500 μm. (F) Statistics of cavity area according to HE staining.

the liposomes. Furthermore, the expression of CD206 was augmented with the decreased expression of CD86. The most CD206 and negligible CD86 expression levels were observed in the bFGF@Lip-Cp&Rp group (Fig. 8D–F). These results show that bFGF@Lip-Cp&Rp facilitates macrophage transformation from M1 to M2, which is beneficial for SCI repair.

3.6. bFGF@Lip-Cp&Rp promotes functional recovery after SCI in rats

Finally, we analyzed motor function recovery after SCI in rats using BBB locomotor scores and walking track analysis. The BBB score (Fig. 9A–C) and footprint (Fig. 9D) studies exhibited that the hind limbs in the 0.9% NaCl group did not recover well. The bFGF@Lip group was slightly improved and the motor function recovery was more significant in the bFGF@Lip-Cp and bFGF@Lip-Rp groups. In addition, the administration of bFGF@Lip-Cp&Rp could markedly improve motor function recovery after SCI. After 28 days of treatment, tissue morphology of the injured spinal cord lesion was examined using HE staining. The 0.9% NaCl group exhibited a large cavity on the injured spinal cord lesion (Fig. 9E–F). However, the cavity area was minimized after bFGF-loaded liposome treatment. The bFGF@Lip-Cp&Rp treatment could significantly reduce cavity formation in the injured spinal cord tissue area. Nissl and NeuN staining were performed to reflect the ability of nerve cells to synthesize proteins. Specifically, we found that Nissl bodies and neurons were relatively more significant and abundant in the bFGF@Lip-Cp&Rp treated group. Intriguingly, fewer and smaller neurons were found in the 0.9% NaCl group (Fig. 10A). Finally, NF-200 (a biomarker of differentiated neurons) and GFAP (a biomarker of reactive astrocytes) immunofluorescence staining was performed to detect the growth of axon at the damaged site. The result revealed that axons at the injured site were almost broken and atrophied in control group, while the liposomes treated group greatly improve axon regeneration, especially for the bFGF@Lip-Cp&Rp treatment (Fig. 10B). In conclusion, these findings imply that the intervention of bFGF@Lip-Cp&Rp improves locomotor recovery and exerts a remarkable neuroprotective effect following SCI.

4. Conclusions

We constructed a bFGF-loaded dual-targeting liposome (bFGF@Lip-Cp&Rp) with injury lesion targeting and BSCB penetrating capability for SCI repair. The injury lesion-targeting effect and BSCB-penetrating capability were verified *in vitro* and *in vivo*. The loaded drug (bFGF) penetrated the BSCB and targeted the lesion area following intravenous injection, subsequently accumulating and remaining in the lesion tissue. Our findings suggested that bFGF@Lip-Cp&Rp repaired the BSCB, enhanced tight-junction protein expression, advanced M1 to M2 macrophage transformation and increased angiogenesis more effectively than unmodified or single-modified liposomes. The spinal cord lesion cavity was smaller, and neuronal and axonal were more preserved and regenerated in the bFGF@Lip-Cp&Rp group. The bFGF@Lip-Cp&Rp

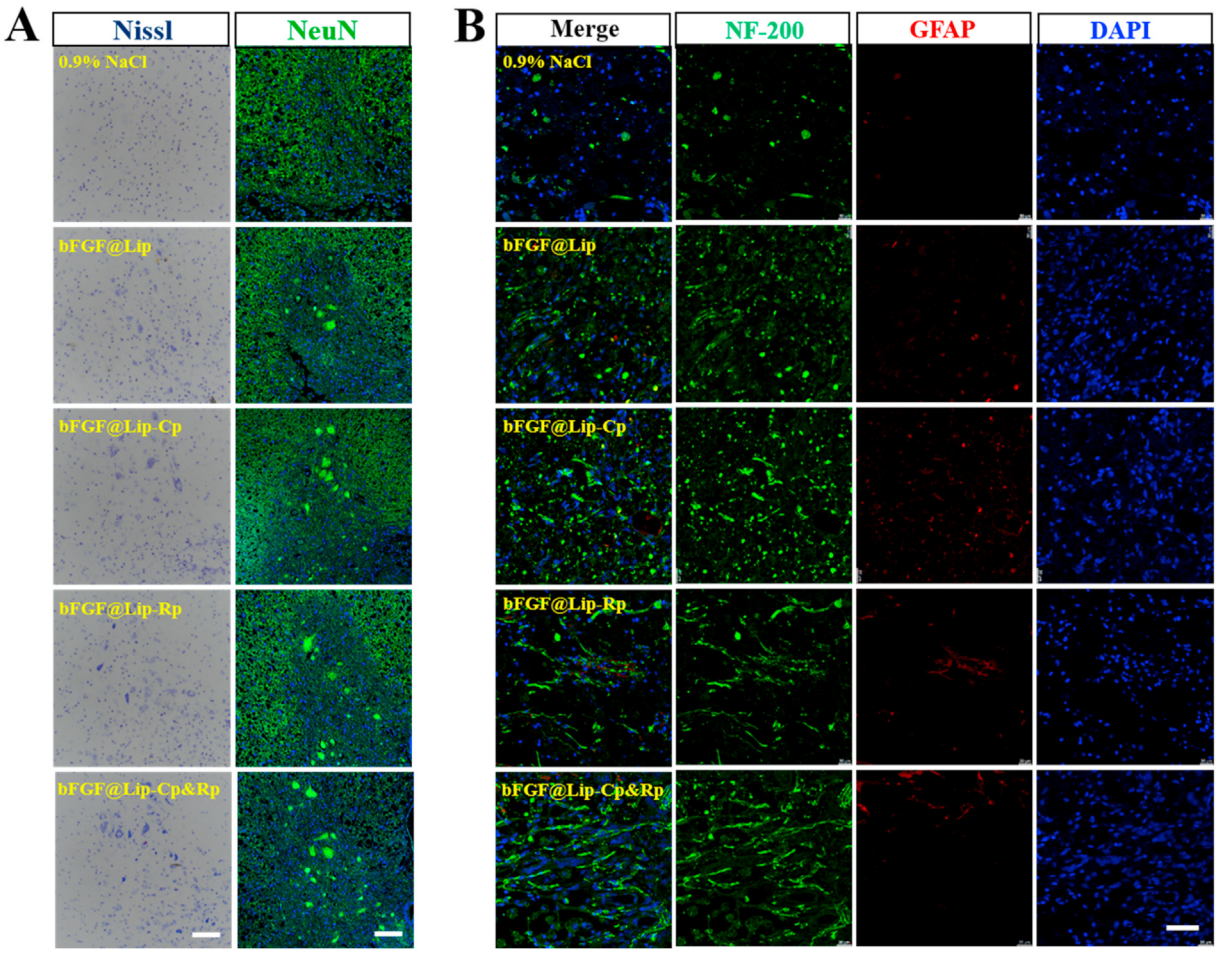

Fig. 10. bFGF@Lip-Cp&Rp inhibited axonal atrophy and promoted axon elongation after SCI. (A) Representative Nissl and NeuN staining images of the groups at 28d after SCI. The scale bar is 100 μm. (B) Representative NF-200 and GFAP staining images of the groups at 28d after SCI. The scale bar is 50 μm.

group facilitated the recovery of limb motor function following SCI. Based on these results, the application of injury lesion targeting and BSCB penetrating drug delivery systems provide promising therapeutic hope for the treatment and management of SCI in the near future.

Credit author Statement

Jian Xiao and Chang Jiang: Conceptualization, Supervision, Funding acquisition; Jie Hu: Investigation, Visualization, Writing-Reviewing and Editing; Fenzan Wu: Resources, Investigation, Visualization, Formal analysis, Writing–Original Draft preparation; Abdullah Al Mamun and Hongyu Zhang: Writing-Reviewing and Editing; Xiaojie Wei, Penghui Wang, Yanhong Yang, Xie Zhang, Yunsen Zhu and Tingting Mo: Resources, Investigation, Funding acquisition. All authors have read and agreed to the published version of the manuscript.

Declaration of competing interest

The authors declare that they have no known competing financial interests or personal relationships that could have appeared to influence the work reported in this paper.

Data availability

Data will be made available on request.

Acknowledgments

This work was supported by the National Natural Science Foundation of China (82172428), Natural Science Foundation of Zhejiang Provincial (LYY21H300003, LQ21H090001), Wenzhou Innovation Team (Growth factor drug development, No. 201801), CAMS Innovation Fund for Medical Sciences (2019-I2M-5–028) and Natural Science Foundation of Ningbo (202003N4041, 202003N4043).

Appendix A. Supplementary data

Supplementary data to this article can be found online at https://doi.org/10.1016/j.mtbio.2023.100546.

References

[1] J. Abbasi, Patients with complete paralysis walk with spinal cord implant, JAMA 327 (2022) 909, https://doi.org/10.1001/jama.2022.2565.
[2] D. Xu, D. Wu, M. Qin, L.R. Nih, C. Liu, Z. Cao, J. Ren, X. Chen, Z. He, W. Yu, J. Guan, S. Duan, F. Liu, X. Liu, J. Li, D. Harley, B. Xu, L. Hou, I.S.Y. Chen, J. Wen, W. Chen, S. Pourtaheri, Y. Lu, Efficient delivery of nerve growth factors to the central nervous system for neural regeneration, Adv. Mater. 31 (2019), e1900727, https://doi.org/10.1002/adma.201900727.
[3] C.M. Zipser, J.J. Cragg, J.D. Guest, M.G. Fehlings, C.R. Jutzeler, A.J. Anderson, A. Curt, Cell-based and stem-cell-based treatments for spinal cord injury: evidence from clinical trials, Lancet Neurol. 21 (2022) 659–670, https://doi.org/10.1016/S1474-4422(21)00464-6.
[4] A.I.R. Maas, W. Peul, C. Thome, Surgical decompression in acute spinal cord injury: earlier is better, Lancet Neurol. 20 (2021) 84–86, https://doi.org/10.1016/S1474-4422(20)30478-6.

[5] J.H. Badhiwala, J.R. Wilson, C.D. Witiw, J.S. Harrop, A.R. Vaccaro, B. Aarabi, R.G. Grossman, F.H. Geisler, M.G. Fehlings, The influence of timing of surgical decompression for acute spinal cord injury: a pooled analysis of individual patient data, Lancet Neurol. 20 (2021) 117–126, https://doi.org/10.1016/S1474-4422(20)30406-3.

[6] K.A. Martin Ginis, H.P. van der Ploeg, C. Foster, B. Lai, C.B. McBride, K. Ng, M. Pratt, C.H. Shirazipour, B. Smith, P.M. Vasquez, G.W. Heath, Participation of people living with disabilities in physical activity: a global perspective, Lancet 398 (2021) 443–455, https://doi.org/10.1016/S0140-6736(21)01164-8.

[7] M.A. Anderson, T.M. O'Shea, J.E. Burda, Y. Ao, S.L. Barlatey, A.M. Bernstein, J.H. Kim, N.D. James, A. Rogers, B. Kato, A.L. Wollenberg, R. Kawaguchi, G. Coppola, C. Wang, T.J. Deming, Z. He, G. Courtine, M.V. Sofroniew, Required growth facilitators propel axon regeneration across complete spinal cord injury, Nature 561 (2018) 396–400, https://doi.org/10.1038/s41586-018-0467-6.

[8] L. Yang, B.M. Conley, S.R. Cerqueira, T. Pongkulapa, S. Wang, J.K. Lee, K.B. Lee, Effective modulation of CNS inhibitory microenvironment using bioinspired hybrid-nanoscaffold-based therapeutic interventions, Adv. Mater. 32 (2020), e2002578, https://doi.org/10.1002/adma.202002578.

[9] S. Ceto, K.J. Sekiguchi, Y. Takashima, A. Nimmerjahn, M.H. Tuszynski, Neural stem cell grafts form extensive synaptic networks that integrate with host circuits after spinal cord injury, Cell Stem Cell 27 (2020) 430–440, https://doi.org/10.1016/j.stem.2020.07.007, e5.

[10] Z. Chen, H. Zhang, C. Fan, Y. Zhuang, W. Yang, Y. Chen, H. Shen, Z. Xiao, Y. Zhao, X. Li, J. Dai, Adhesive, stretchable, and spatiotemporal delivery fibrous hydrogels harness endogenous neural stem/progenitor cells for spinal cord injury repair, ACS Nano 16 (2022) 1986–1998, https://doi.org/10.1021/acsnano.1c06892.

[11] W. Guo, X. Zhang, J. Zhai, J. Xue, The roles and applications of neural stem cells in spinal cord injury repair, Front. Bioeng. Biotechnol. 10 (2022), 966866, https://doi.org/10.3389/fbioe.2022.966866.

[12] Z. Alvarez, A.N. Kolberg-Edelbrock, I.R. Sasselli, J.A. Ortega, R. Qiu, Z. Syrgiannis, P.A. Mirau, F. Chen, S.M. Chin, S. Weigand, E. Kiskinis, S.I. Stupp, Bioactive scaffolds with enhanced supramolecular motion promote recovery from spinal cord injury, Science 374 (2021) 848–856, https://doi.org/10.1126/science.abh3602.

[13] T. Yuan, Y. Shao, X. Zhou, Q. Liu, Z. Zhu, B. Zhou, Y. Dong, N. Stephanopoulos, S. Gui, H. Yan, D. Liu, Highly permeable DNA supramolecular hydrogel promotes neurogenesis and functional recovery after completely transected spinal cord injury, Adv. Mater. 33 (2021), e2102428, https://doi.org/10.1002/adma.202102428.

[14] K. Xi, Y. Gu, J. Tang, H. Chen, Y. Xu, L. Wu, F. Cai, L. Deng, H. Yang, Q. Shi, W. Cui, L. Chen, Microenvironment-responsive immunoregulatory electrospun fibers for promoting nerve function recovery, Nat. Commun. 11 (2020) 4504, https://doi.org/10.1038/s41467-020-18265-3.

[15] X. Hu, R. Li, Y. Wu, Y. Li, X. Zhong, G. Zhang, Y. Kang, S. Liu, L. Xie, J. Ye, J. Xiao, Thermosensitive heparin-poloxamer hydrogel encapsulated bFGF and NGF to treat spinal cord injury, J. Cell Mol. Med. 24 (2020) 8166–8178, https://doi.org/10.1111/jcmm.15478.

[16] J. Shang, H. Qiao, P. Hao, Y. Gao, W. Zhao, H. Duan, Z. Yang, X. Li, bFGF-sodium hyaluronate collagen scaffolds enable the formation of nascent neural networks after adult spinal cord injury, J. Biomed. Nanotechnol. 15 (2019) 703–716, https://doi.org/10.1166/jbn.2019.2732.

[17] X. Yu, A.H. Biedrzycki, A.S. Khalil, D. Hess, J.M. Umhoefer, M.D. Markel, W.L. Murphy, Nanostructured mineral coatings stabilize proteins for therapeutic delivery, Adv. Mater. 29 (2017), https://doi.org/10.1002/adma.201701255.

[18] T.H. Nguyen, S.H. Kim, C.G. Decker, D.Y. Wong, J.A. Loo, H.D. Maynard, A heparin-mimicking polymer conjugate stabilizes basic fibroblast growth factor, Nat. Chem. 5 (2013) 221–227, https://doi.org/10.1038/nchem.1573.

[19] W. Deng, F. Shao, Q. He, Q. Wang, W. Shi, Q. Yu, X. Cao, C. Feng, S. Bi, J. Chen, P. Ma, Y. Li, A. Gong, S. Tong, J. Yu, M. Spector, X. Xu, Z. Zhang, EMSCs build an all-in-one niche via cell-cell lipid raft assembly for promoted neuronal but suppressed astroglial differentiation of neural stem cells, Adv. Mater. 31 (2019), e1806861, https://doi.org/10.1002/adma.201806861.

[20] A. Canales, S. Park, A. Kilias, P. Anikeeva, Multifunctional fibers as tools for neuroscience and neuroengineering, Acc. Chem. Res. 51 (2018) 829–838, https://doi.org/10.1021/acs.accounts.7b00558.

[21] H.L. Xu, P.P. Chen, D.L. ZhuGe, Q.Y. Zhu, B.H. Jin, B.X. Shen, J. Xiao, Y.Z. Zhao, Liposomes with silk fibroin hydrogel core to stabilize bFGF and promote the wound healing of mice with deep second-degree scald, Adv. Healthc. Mater. 6 (2017), https://doi.org/10.1002/adhm.201700344.

[22] Y.Z. Zhao, M. Lin, Q. Lin, W. Yang, X.C. Yu, F.R. Tian, K.L. Mao, J.J. Yang, C.T. Lu, H.L. Wong, Intranasal delivery of bFGF with nanoliposomes enhances in vivo neuroprotection and neural injury recovery in a rodent stroke model, J. Contr. Release 224 (2016) 165–175, https://doi.org/10.1016/j.jconrel.2016.01.017.

[23] H. Wang, S. Zhang, Z. Liao, C. Wang, Y. Liu, S. Feng, X. Jiang, J. Chang, PEGlated magnetic polymeric liposome anchored with TAT for delivery of drugs across the blood-spinal cord barrier, Biomaterials 31 (2010) 6589–6596, https://doi.org/10.1016/j.biomaterials.2010.04.057.

[24] J.Y. Tyler, X.M. Xu, J.X. Cheng, Nanomedicine for treating spinal cord injury, Nanoscale 5 (2013) 8821–8836, https://doi.org/10.1039/c3nr00957b.

[25] H. Peluffo, U. Unzueta, M.L. Negro-Demontel, Z. Xu, E. Vaquez, N. Ferrer-Miralles, A. Villaverde, BBB-targeting, protein-based nanomedicines for drug and nucleic acid delivery to the CNS, Biotechnol. Adv. 33 (2015) 277–287, https://doi.org/10.1016/j.biotechadv.2015.02.004.

[26] A. Chakraborty, A.J. Ciciriello, C.M. Dumont, R.M. Pearson, Nanoparticle-based delivery to treat spinal cord injury—a mini-review, AAPS PharmSciTech 22 (2021) 1–9.

[27] S.L. Lindsay, G.A. McCanney, A.G. Willison, S.C. Barnett, Multi-target approaches to CNS repair: olfactory mucosa-derived cells and heparan sulfates, Nat. Rev. Neurol. 16 (2020) 229–240.

[28] A.P. Tran, P.M. Warren, J. Silver, The biology of regeneration failure and success after spinal cord injury, Physiol. Rev. 98 (2018) 881–917, https://doi.org/10.1152/physrev.00017.2017.

[29] H.H. Park, Y.M. Kim, L.T. Anh Hong, H.S. Kim, S.H. Kim, X. Jin, D.H. Hwang, M.J. Kwon, S.C. Song, B.G. Kim, Dual-functional hydrogel system for spinal cord regeneration with sustained release of arylsulfatase B alleviates fibrotic microenvironment and promotes axonal regeneration, Biomaterials 284 (2022), 121526, https://doi.org/10.1016/j.biomaterials.2022.121526.

[30] X. Sun, H. Liu, Z. Tan, Y. Hou, M. Pang, S. Chen, L. Xiao, Q. Yuan, B. Liu, L. Rong, L. He, Remodeling microenvironment for endogenous repair through precise modulation of chondroitin sulfate proteoglycans following spinal cord injury, Small (2022), e2205012, https://doi.org/10.1002/smll.202205012.

[31] N. Mukherjee, S. Nandi, S. Garg, S. Ghosh, S. Ghosh, R. Samat, S. Ghosh, Targeting chondroitin sulfate proteoglycans: an emerging therapeutic strategy to treat CNS injury, ACS Chem. Neurosci. 11 (2020) 231–232, https://doi.org/10.1021/acschemneuro.0c00004.

[32] A.P. Mann, P. Scodeller, S. Hussain, J. Joo, E. Kwon, G.B. Braun, T. Mölder, Z.-G. She, V.R. Kotamraju, B. Ranscht, A peptide for targeted, systemic delivery of imaging and therapeutic compounds into acute brain injuries, Nat. Commun. 7 (2016) 1–11.

[33] J. Wang, D. Li, C. Liang, C. Wang, X. Zhou, L. Ying, Y. Tao, H. Xu, J. Shu, X. Huang, Scar tissue-targeting polymer micelle for spinal cord injury treatment, Small 16 (8) (2020), 1906415.

[34] Q. Wang, H. Zhang, H. Xu, Y. Zhao, Z. Li, J. Li, H. Wang, D. Zhuge, X. Guo, H. Xu, S. Jones, X. Li, X. Jia, J. Xiao, Novel multi-drug delivery hydrogel using scar-homing liposomes improves spinal cord injury repair, Theranostics 8 (2018) 4429–4446, https://doi.org/10.7150/thno.26717.

[35] Y.H. Song, N.K. Agrawal, J.M. Griffin, C.E. Schmidt, Recent advances in nanotherapeutic strategies for spinal cord injury repair, Adv. Drug Deliv. Rev. 148 (2019) 38–59, https://doi.org/10.1016/j.addr.2018.12.011.

[36] M.J. Majcher, A. Babar, A. Lofts, A. Leung, X. Li, F. Abu-Hijleh, N.M.B. Smeets, R.K. Mishra, T. Hoare, In situ-gelling starch nanoparticle (SNP)/O-carboxymethyl chitosan (CMCh) nanoparticle network hydrogels for the intranasal delivery of an antipsychotic peptide, J. Contr. Release 330 (2021) 738–752, https://doi.org/10.1016/j.jconrel.2020.12.050.

[37] K. Shen, G. Sun, L. Chan, L. He, X. Li, S. Yang, B. Wang, H. Zhang, J. Huang, M. Chang, Z. Li, T. Chen, Anti-inflammatory nanotherapeutics by targeting matrix metalloproteinases for immunotherapy of spinal cord injury, Small 17 (2021), e2102102, https://doi.org/10.1002/smll.202102102.

[38] A.D. Tagalakis, V. Jayarajan, R. Maeshima, K.H. Ho, F. Syed, L.P. Wu, A.M. Aldossary, M.M. Munye, T. Mistry, O.K. Ogunbiyi, A. Sala, J.F. Standing, S.M. Moghimi, A.W. Stoker, S.L. Hart, Integrin-targeted, short interfering RNA nanocomplexes for neuroblastoma tumor-specific delivery achieve MYCN silencing with improved survival, Adv. Funct. Mater. 31 (2021), 2104843, https://doi.org/10.1002/adfm.202104843.

[39] J. Li, J. Wei, Y. Wan, X. Du, X. Bai, C. Li, Y. Lin, Z. Liu, M. Zhou, Z. Zhong, TAT-modified tetramethylpyrazine-loaded nanoparticles for targeted treatment of spinal cord injury, J. Contr. Release 335 (2021) 103–116.

[40] B. Surnar, U. Basu, B. Banik, A. Ahmad, B. Marples, N. Kolishetti, S. Dhar, Nanotechnology-mediated crossing of two impermeable membranes to modulate the stars of the neurovascular unit for neuroprotection, Proc. Natl. Acad. Sci. USA 115 (2018) E12333–E12342.

[41] J. Wu, H. Jiang, Q. Bi, Q. Luo, J. Li, Y. Zhang, Z. Chen, C. Li, Apamin-mediated actively targeted drug delivery for treatment of spinal cord injury: more than just a concept, Mol. Pharm. 11 (2014) 3210–3222.

[42] L. Jiang, S. Zhou, X. Zhang, C. Li, S. Ji, H. Mao, X. Jiang, Mitochondrion-specific dendritic lipopeptide liposomes for targeted sub-cellular delivery, Nat. Commun. 12 (2021) 1–12.

[43] J. Li, J. Wei, Y. Wan, X. Du, X. Bai, C. Li, Y. Lin, Z. Liu, M. Zhou, Z. Zhong, TAT-modified tetramethylpyrazine-loaded nanoparticles for targeted treatment of spinal cord injury, J. Contr. Release 335 (2021) 103–116, https://doi.org/10.1016/j.jconrel.2021.05.016.

[44] S. Futaki, I. Nakase, Cell-surface interactions on arginine-rich cell-penetrating peptides allow for multiplex modes of internalization, Acc. Chem. Res. 50 (2017) 2449–2456, https://doi.org/10.1021/acs.accounts.7b00221.

[45] M. Li, X. Tang, X. Liu, X. Cui, M. Lian, M. Zhao, H. Peng, X. Han, Targeted miR-21 loaded liposomes for acute myocardial infarction, J. Mater. Chem. B 8 (2020) 10384–10391, https://doi.org/10.1039/d0tb01821j.

[46] Y. Liu, X. Wang, J. Li, J. Tang, B. Li, Y. Zhang, N. Gu, F. Yang, Sphingosine 1-phosphate liposomes for targeted nitric oxide delivery to mediate anticancer effects against brain glioma tumors, Adv. Mater. 33 (2021), e2101701, https://doi.org/10.1002/adma.202101701.

[47] Y. Lin, Y. Wan, X. Du, J. Li, J. Wei, T. Li, C. Li, Z. Liu, M. Zhou, Z. Zhong, TAT-modified serum albumin nanoparticles for sustained-release of tetramethylpyrazine and improved targeting to spinal cord injury, J. Nanobiotechnol. 19 (2021) 28, https://doi.org/10.1186/s12951-020-00766-4.

[48] W. Fenzan, Z. Yan, W. Wanqing, Y. Yanhong, H. Jie, M. Yuqin, S. Changmin, X. Jian, Multifunctional inverse opal film as a responsive drug carrier for spinal cord injury repair, Chem. Eng. J. 436 (2022), 135256, https://doi.org/10.1016/j.cej.2022.135256.

[49] Z. Liu, Y. Jiao, Q. Chen, Y. Li, J. Tian, Y. Huang, M. Cai, D. Wu, Y. Zhao, Two sigma and two mu class genes of glutathione S-transferase in the waterflea Daphnia pulex: molecular characterization and transcriptional response to nanoplastic exposure,

Chemosphere 248 (2020), 126065, https://doi.org/10.1016/j.chemosphere.2020.126065.

[50] Y. Feng, Q. Li, D. Wu, Y. Niu, C. Yang, L. Dong, C. Wang, A macrophage-activating, injectable hydrogel to sequester endogenous growth factors for in situ angiogenesis, Biomaterials 134 (2017) 128–142, https://doi.org/10.1016/j.biomaterials.2017.04.042.

[51] L. Li, J. Mu, Y. Zhang, C. Zhang, T. Ma, L. Chen, T. Huang, J. Wu, J. Cao, S. Feng, Y. Cai, M. Han, J. Gao, Stimulation by exosomes from hypoxia preconditioned human umbilical vein endothelial cells facilitates mesenchymal stem cells angiogenic function for spinal cord repair, ACS Nano (2022), https://doi.org/10.1021/acsnano.2c02898.

[52] J. Van Broeckhoven, D. Sommer, D. Dooley, S. Hendrix, A. Franssen, Macrophage phagocytosis after spinal cord injury: when friends become foes, Brain 144 (2021) 2933–2945, https://doi.org/10.1093/brain/awab250.

[53] G.Y. Xu, S. Xu, Y.X. Zhang, Z.Y. Yu, F. Zou, X.S. Ma, X.L. Xia, W.J. Zhang, J.Y. Jiang, J. Song, Cell-free extracts from human fat tissue with a hyaluronan-based hydrogel attenuate inflammation in a spinal cord injury model through M2 microglia/microphage polarization, Small 18 (2022), e2107838, https://doi.org/10.1002/smll.202107838.